# Microscopic dynamics of $AC_{60}$ compounds in the plastic, polymer, and dimer phases investigated by inelastic neutron scattering

H. Schober and A. Tölle
*Institut Laue-Langevin, F-38042 Grenoble, France*

B. Renker, R. Heid, and F. Gompf
*INFP, Forschungszentrum Karlsruhe, D-76021 Karlsruhe, Federal Republic of Germany*

(Received 29 July 1996; revised manuscript received 28 April 1997)

We present inelastic neutron-scattering results for $AC_{60}$ ($A$=K,Rb,Cs) compounds. The spectra of the high-temperature fcc phases strongly resemble the ones of pristine $C_{60}$ in the plastic phase. At equal temperatures we find identical rotational diffusion constants for pristine $C_{60}$ and $Rb_1C_{60}$ ($D_r$=2.4 $10^{10}$ $s^{-1}$ at 400 K). The changes taking place in the inelastic part of the spectra on cooling $AC_{60}$ indicate the formation of strong intermolecular bonds. The buildup of intensities in the gap region separating internal and external vibrations in pure $C_{60}$ is the most prominent signature of this transition. The spectra of the low-temperature phases depend on their thermal history. The differences can be explained by the formation of a polymer phase (upon slow cooling from the fcc phase) and a dimer phase (upon fast cooling), respectively. The experimental data are analyzed on the basis of lattice dynamical calculations. The density-of-states are well modeled assuming a [2+2] bond for the polymer and a single intercage bond for the dimer. Indications for different intercage bonding are also found in the internal mode spectra, which, on the other hand, react only weakly to the charge transfer. The dimer phase is metastable and converts into the polymer phase with a strongly temperature-dependent time constant. The transition from the polymer to the fcc phase is accompanied by inelastic precursor effects which are interpreted as the signature of inhomogeneities arising from plastic monomer regions embedded in the polymer phase. In the polymer phase $AC_{60}$ compounds show strong anharmonic behavior in the low-temperature region. The possible connection with the metal-to-insulator transition is discussed. [S0163-1829(97)04834-0]

## I. INTRODUCTION

Among the alkali-metal-doped $C_{60}$ crystals the $AC_{60}$ compositions ($A$=K,Rb,Cs) show exceptionally rich phase diagrams due to solid-state chemical reactions. These reactions lead to the formation of strong covalent bonds between the $C_{60}$ molecules in contrast to the usual intermolecular bonding via van der Waals and Coulomb forces (e.g., in $A_3C_{60}$ and $A_6C_{60}$ compounds). In order to understand the physical properties of these fulleride phases a large variety of investigational techniques have been applied. The structural parameters have been resolved using x-ray diffraction.[1–6] At elevated temperatures ($\approx$ 450 K) the $AC_{60}$ compounds crystallize in a fcc structure with the alkali ions fully occupying the octahedral vacancy sites.[5]

Upon slow cooling the fcc structure converts into an orthorhombic structure, in which the $C_{60}$ molecules combine to form linear polymer chains.[1,2,7] The polymer phase is thermodynamically stable at room temperature and, in contrast to other alkali fullerides, may be exposed to air. In $K_1C_{60}$ the situation is more complex than outlined above due to the fact that the fcc phase becomes thermodynamically unstable before the polymer formation sets in. This leads to the intercalation of an intermediate phase which is thought to consist of a continuous lattice featuring $K_3C_{60}$ and K-free regions.[5] Spin susceptibility, optical conductivity,[8] NMR,[9,10] and resistivity measurements[5] identify the polymer phases at room temperature as metallic. The details of the electronic properties depend crucially on the alkali ion. For $Rb_1C_{60}$ and $Cs_1C_{60}$ a metal-insulator transition (MIT) is observed at 50 and 40 K, respectively.[8] In the case of $K_1C_{60}$ the situation is less clear.[11] While electron spin resonance (ESR) experiments seem to indicate that $K_1C_{60}$ stays metallic down to lowest temperatures resistivity measurements come up with indications for a metal-to-semiconductor transition near 50 K. The experimental observation of a MIT in $Rb_1C_{60}$ and $Cs_1C_{60}$ spurred several theoretical studies. First-principle density functional calculations[12] favor a three-dimensional (3D) antiferromagnetically ordered ground state, while a semiempirical tight-binding model[13] comes up with a critical dependence of the electronic behavior on the degree of $\pi$ conjugation present in the inter-$C_{60}$ bonds. So far, the experimental evidence does not permit us to draw a definite picture of the electronic ground state in the orthorhombic phase. While the muon-spin-relaxation (MSR) measurements on $Rb_1C_{60}$ done by Uemura *et al.*[14] are interpreted as being compatible with a spin-density-wave state, MacFarlane *et al.*,[15] using the same experimental technique, claim that the magnetic structure must be more disordered. The same conclusion is reached by Cristofolini *et al.*[16] investigating $Cs_1C_{60}$ with MSR. Neutron-diffraction experiments on $Rb_1C_{60}$ powder at 100 and 10 K do not show differences which could be interpreted as signatures of 3D magnetic ordering.[17] The NMR data by Brouet *et al.*[18] support antiferromagnetic fluctuations up to room temperature and the occurence of an antiferromagnetic spin-flop phase below 25 K.

 

If the $AC_{60}$ crystals are sufficiently rapidly quenched from the high-temperature fcc phase the polymer formation is suppressed. The diffraction patterns of this new phase signal the existence of $(C_{60})_2^{-2}$ dimers.[3,4,6] The electronic system of the dimer phase shows a transition from diamagnetic to paramagnetic response.[4] At least in $K_1C_{60}$ the dimer phase seems to convert into the polymer phase via an intermediate fcc phase.[4]

Indirect confirmation of the polymer and dimer formation has been provided from optical spectroscopy. Raman[19,20] and infrared measurements[20] show strong variations of the $C_{60}$ intramolecular excitation spectrum which can only be understood by a breakdown of the icosahedral symmetry caused by the formation of inter-$C_{60}$ covalent bonds. In the polymer these bonds are thought to correspond to a [2+2] cycloaddition involving double (6,6) bonds on adjacent $C_{60}$ molecules in analogy to the photo-[21] and pressure-induced[22] polymerization of pristine $C_{60}$ while the type of bonding seems to depend crucially on the charge state in the case of the dimer.[23,6]

The present study intends to contribute towards a deeper understanding of the dynamical processes taking place in these fascinating materials. Inelastic neutron scattering (INS) provides detailed information on the excitation spectra over a large dynamical range. In contrast to optical measurements neutron experiments are not restricted to the vicinity of the zone center. As, in addition, all excitations are allowed, we are able to extract the vibrational density-of-states (VDOS). The most direct information about the bonding of $C_{60}$ molecules is contained in the low-frequency part of the spectra. Vanishing intensities in the region between 8 and 33 meV in pristine $C_{60}$[24] reflect the fact that we are dealing with two different energy scales. These scales are set by weak intermolecular van der Waals and strong intramolecular covalent C-C bonds, respectively. This separation of scales breaks down upon polymerization or dimerization resulting in a filling of the gap. The spectral distribution of the gap intensities is closely related to the particular bonding. Quantitative information about the bond strengths can be obtained by a comparison with model calculation. The changes of the spectra with temperature shed light on the phase transition mechanisms. Precursors of these transitions are, in particular, to be expected in the Debye region. As the transitions are associated with a change in orientational ordering — such as in pristine $C_{60}$[25]— libronic excitations may be expected to soften when approaching $T_c$.

The paper is structured as follows. In Sec. II we give details about sample preparation, experimental setup, and data analysis. The discussion of the experimental results starts with the lattice dynamics of the fcc, polymer, and dimer phase. External modes (Sec. III) and internal modes (Sec. IV) will be treated separately. The insight gained there then allows us to study the structural phase transitions in Sec. V. The final part of the paper is devoted to the dynamics at low temperatures and its possible connection with the MIT.

## II. EXPERIMENT

### A. Sample preparation

$AC_{60}$ samples can be obtained by the reaction of alkali vapor with $C_{60}$ at elevated temperatures. We followed a slightly different route, producing homogeneous $AC_{60}$ samples by annealing stoichiometric quantities of $C_{60}$ and $A_6C_{60}$ powders at T $\approx$ 650 K for several days. Despite the fact that $A_1C_{60}$ compounds are stable with respect to air exposure the samples were handled in an inert gas atmosphere and sealed into air-tight, cylindrical aluminium containers. The $Rb_1C_{60}$ and $Cs_1C_{60}$ polymer phases were produced by a slow cooling to room temperature (RT). The phase purity was checked by x-ray diffraction. Sample quantities of the order of 1 g were investigated. To obtain the dimer phases the samples were quenched from 450 to 77 K and then immediately transferred into the cryostat of the instrument. During the transfer the temperature was continuously monitored and at no time exceeded 200 K.

### B. Spectrometers

The INS experiments were done using two spectrometers: the cold neutron time-of-flight instrument IN6 at the high-flux reactor of the Institute Laue-Langevin and the thermal neutron time-of-flight instrument DN6 at the Siloé reactor of the CENG, both situated in Grenoble, France.

The instrument IN6 was chosen for several reasons. Due to its focusing techniques it provides a very high flux allowing for a large number of short runs at various temperatures. We thus are able to follow the different transformations and their precursors in great detail. The energy region of particular interest between 0.5 meV and the first intra-$C_{60}$ excitation around 30 meV can be covered in neutron energy gain mode (up-scattering) down to temperatures of about 200 K. At the same time the energy resolution is sufficiently good to observe in detail the softening of modes in the Debye region. The incident energy $E_i$ was chosen to be 4.75 meV. Data were collected in 235 $^3$He counters covering the angular range from 10 to 113°. These angles translate into an elastic wavevector range of 0.3 Å$^{-1} \leqslant Q_{\rm el} \leqslant$ 2.6 Å$^{-1}$. The elastic resolution amounts to 170 $\mu$eV full width at half maximum (FWHM) when time-focusing on the elastic line. Both time-focusing on the elastic line and in the inelastic region was used to optimized resolution as a function of energy transfer.

The thermal instrument DN6 was used in order to complement the results of IN6 for larger $Q$ values (up to 7 Å$^{-1}$ at $\hbar\omega = 0$) and also to investigate the internal mode spectrum with better resolution. The 304 $^3$He counters were positioned such as to cover the scattering angles from 24° to 100°. Experiments with three different incident energies $E_i$ were performed: 17.4 meV ($\delta E_{\rm elastic} \approx$ 0.8 meV FWHM) using PG002, 45.0 meV ($\delta E_{\rm elastic} \approx$ 3.0 meV FWHM) using CU111, 70.0 meV ($\delta E_{\rm elastic} \approx$ 4.5 meV FWHM) using PG004. Both the neutron energy gain and loss (down-scattering) sides of the spectra were exploited.

### C. Data analysis

The time-of-flight spectra are corrected for background scattering and are properly normalized to both the incoming flux and a vanadium standard. After corrections for the energy dependence of the detector efficiency the scattering law $S(2\theta,\omega)$ is obtained. $S(2\theta,\omega)$ can be converted into $S(Q,\omega)$ using an adapted interpolation scheme.

The vibrational density-of-states (VDOS) is a particularly useful quantity for studying lattice dynamics. The VDOS is

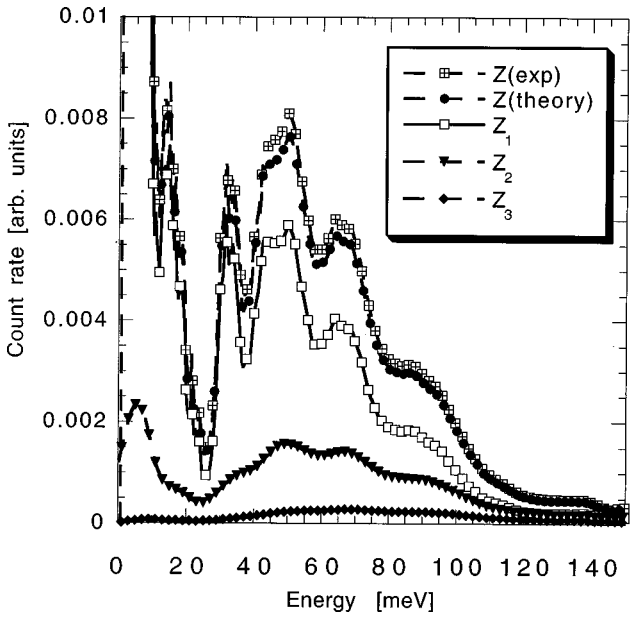


FIG. 1. Inelastic spectrum of $Rb_1C_{60}$ at 350 K ($E_i$=4.75 meV) after summation over detectors and conversion to energy. $Z$(exp): experimental result; $Z$(theory): spectrum calculated using the self-consistently determined $G(\omega)$ as input; $Z_n$: calculated $n$-phonon contribution to the spectrum. The mean square displacement is $\langle u^2\rangle = 0.038$ Å$^2$.

directly related to the one phonon part of the incoherent scattering function.[26] As, however, both the alkali and carbon atoms are coherent scatterers we are obliged to invoke the incoherent approximation[27] in order to extract the VDOS from the INS spectra, i.e., we assume that

$$\int_{Q_{\min}}^{Q_{\max}} \left(\frac{d^2\sigma}{d(\hbar\omega)d\Omega}\right)_{\text{coh}} dQ \approx \int_{Q_{\min}}^{Q_{\max}} \left(\frac{d^2\sigma}{d(\hbar\omega)d\Omega}\right)_{\text{inc}} dQ \tag{1}$$

for a sufficiently large $Q$ sampling. The right-hand side refers to a hypothetical incoherent sample. The $G(\omega)$ obtained from the INS data is a generalized vibrational density-of-states (GDOS), which differs from the actual VDOS in that the contributions of the different ions are weighted with their scattering powers $\sigma/M$. Multiphonon contributions to $S(Q,\omega)$ are determined self-consistently. It turns out that the multiphonon contributions to the spectra are negligible in the low-frequency intermolecular region ($\approx$2% at 4 meV and 350 K for the IN6 data.) They, however, become important for the molecular excitations at higher energies due to the increase in $Q$. For example, at 350 K the multiphonon contributions in the IN6 spectra are of the same order of magnitude as the one-phonon part for energies above 100 meV (see Fig. 1). As the multiphonon contributions involve a folding of the density-of-states they contribute a broad background distribution which hardly alters the peak positions.

The validity of the incoherent approximation can be checked by comparing $G(\omega)$ as obtained from different sampling regions in $Q$ space. For $Rb_1C_{60}$ we find that as long as $Q_{\max}(\omega)$ exceeds 3.0 Å$^{-1}$ $G(\omega)$ is only weakly dependent on the $Q$ range explored (apart from changes which can be traced back to differences in energy resolution). In the case of the IN6 experiments using $E_i$= 4.75 meV this condition is

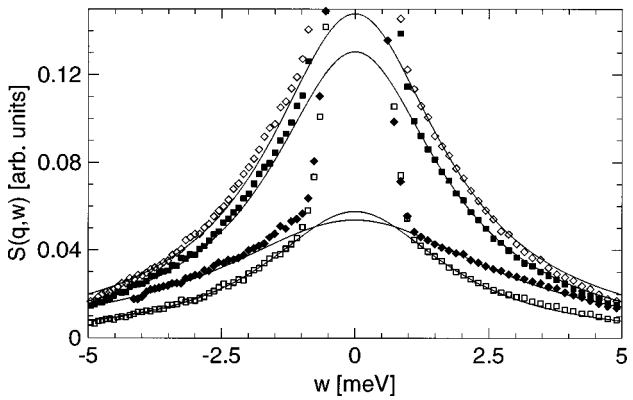


FIG. 2. Symmetrized $S(Q,\omega)$ for $Rb_1C_{60}$ at 400 K in the quasielastic region ($E_i$=17.4 meV). Points correspond to the experimental data: open squares 2.5 Å$^{-1}$, full squares 3.0 Å$^{-1}$, open lotzgens 3.5 Å$^{-1}$, and full lotzgens 4.0 Å$^{-1}$. The lines correspond to Lorentzians (see Eq. 3) convoluted with the instrument resolution.

fullfilled for $\hbar\omega > 2$ meV. The reason for this behavior is to be found in the rather peculiar shape of the $C_{60}$ molecule, reminiscent of a hollow sphere, leading to dynamical form factors for the librational modes[28,29] which are practically zero for $Q$ values smaller than 2.5 Å$^{-1}$. When performing the incoherent approximation a too restricted $Q$ range, therefore, excludes the libronic excitations[30] from the obtained GDOS.

$G(\omega)$ is always a well-defined function and offers a concise way of presenting the experimental data which accounts for the Debye-Waller and Bose factor variations and corrects for multiphonon contributions. The incoherent approximation enters only when identifying $G(\omega)$ with the actual GDOS.

A large part of the discussion will be done presenting the data in the form of $\omega^{-1}\chi''[\omega]$, where $\chi''[\omega]$ denotes the generalized susceptibility. To improve the data statistics integration is again carried out over $Q$. We would like to point out that due to this $Q$ integration $\omega^{-1}\chi''[\omega]$ is instrument dependent, which poses no problem for the relative comparisions we will do. To a first approximation the quantity $\omega^{-1}\chi''[\omega]$ is proportional to $\omega^2 G(\omega)$ as Debye-Waller and multiphonon corrections partially compensate each other.[31] $\omega^{-1}\chi''[\omega]$ is in direct connection with the actual experimental data

$$\omega^{-1}\chi''[\omega] \propto T^{-1}\mathrm{S}(\omega) \quad \text{for } \hbar\omega << k_b T. \tag{2}$$

The relative errors in the data are thus preserved. In addition, $\omega^{-1}\chi''[\omega]$ is well suited even for systems featuring diffusion processes while the concept of a density-of-states becomes doubtful in this case.

## III. MICROSCOPIC DYNAMICS IN THE LOW-FREQUENCY REGION

### A. fcc phase

The high-temperature ($T$>400 K) INS spectrum of $Rb_1C_{60}$ resembles strongly the one of pristine $C_{60}$, i.e., it features broad quasielastic contributions at low frequencies separated from the spectrum of intramolecular vibrations by a well-pronounced gap. In Fig. 2 we show typical spectra of

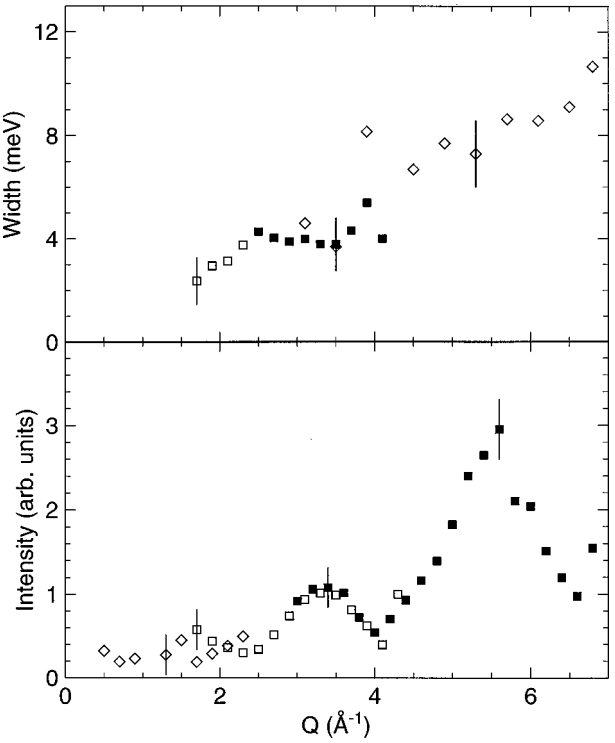


FIG. 3. Pseudolinewidth $\Gamma(Q)$ and intensity $I(Q)$ for $Rb_1C_{60}$ at 400 K as obtained by fitting Lorentzians to the experimental data [see Eq. (3) and Fig. 2]. The experimental results agree well with the predictions of a rotational diffusion model. The diffusion constant comes out as $D_r = 2.4\ 10^{10}\ s^{-1}$. The different symbols correspond to measurements using IN6 at 4.75 meV (open lotzgens), DN6 at 17.4 meV (open squares), and DN6 at 45 meV (full squares).

the quasielastic region. For a given $Q$ the symmetrized scattering law can be well parametrized by single Lorenzian functions (folded with the instrument resolution):

$$S_L(Q,\omega)=\frac{I}{\pi}\frac{\Gamma/2}{\omega^2+(\Gamma/2)^2}. \tag{3}$$

The so obtained intensities $I(Q)$ and pseudolinewidths $\Gamma(Q)$ of the quasielastic signal are shown in Fig. 3. Data from three experimental setups (IN6 at 4.75 meV, DN6 at 17.4 and 45.0 meV) have been combined in order to cover the wave vector range from $0.3\ \text{Å}^{-1} \leqslant Q \leqslant 7\ \text{Å}^{-1}$. The mapping of the data was achieved by a vanadium standard. The results agree well with the $I(Q)$ and $\Gamma(Q)$ obtained by fitting Eq. (3) to the exact theoretical expression of a rotational diffusion model.[25,29] The only free parameter of such a statistical model is the diffusion constant, which becomes for the present case $D_r = 2.4\ 10^{10}\ s^{-1}$ ($Rb_1C_{60}$ at 400 K). This means that, as in pristine $C_{60}$ above its sc $\rightarrow$ fcc transition, we are dealing with a plastic crystal phase. For comparison, $D_r = 1.8\ 10^{10}\ s^{-1}$ for pristine $C_{60}$ at 300 K. To check whether the presence of the Rb ions in $Rb_1C_{60}$ has any influence on the rotational relaxation time $\tau_r$ we repeated the measurements using $C_{60}$ powder. At 400 K the quasielastic part of the spectra of $C_{60}$ and $Rb_1C_{60}$ turns out to be indistinguishable within the experimental errors and apart from the small extra scattering from the Rb ions the elastic signals have exactly the same absolute strength.

It has been shown recently[32] by INS experiments on single crystals of $C_{60}$ that short-range orientational order may persist above the sc $\rightarrow$ fcc transition, although the powder results agree well with the predictions of a continuous rotational diffusion model.[33,50] Short-range orientational order in $Rb_1C_{60}$ can be ruled out on the basis of the elastic part of the powder spectra. The coherence length of about 40 Å found just above $T_c$ in pristine $C_{60}$ diminishes rapidly with temperature. As observed in the temperature range from 260 to 400 K this loss of orientational order leads to a decline of the elastic intensities beyond what is expected from the decrease of the vibrational Debye-Waller factor. At 400 K orientational order can be excluded in fcc $C_{60}$. Therefore, if short-range orientational order were present in fcc $Rb_1C_{60}$ then the absolute strength of the elastic signal should exceed the one of $C_{60}$. This, however, is not observed experimentally.[34]

The fast reorientation of the $C_{60}$ molecules in the absence of short-range orientational order may strongly favor the polymerization process by bringing together $C_{60}$ molecules in all possible relative configurations. Among those configurations the ones featuring parallel (6,6) bonds then can evolve into the formation of covalent [2+2] cycloaddition bonds.[35] This scenario is the more intriguing as the fast rotation rates in fcc $AC_{60}$ coincide with rather short inter-$C_{60}$ distances.[3] The distances found in $AC_{60}$ at 420 K are close to the ones in pristine $C_{60}$ near the order-disorder transition,[36] probably due to the presence of Coulomb attractions in $AC_{60}$. The essential difference leading to the polymerization in $AC_{60}$ is not of dynamical but quantum-chemical nature. The energy barriers for polymer formation are too high for uncharged $C_{60}$ molecules in their respective electronic ground states.

### B. Polymer phase

Cooling $Rb_1C_{60}$ samples slowly from the high-temperature phase leads to the formation of one-dimensional polymer chains. Following the discovery[21] of photopolymerization in pristine $C_{60}$ several theoretical calculations for the zone center modes of neutral $C_{60}$ chains were performed.[37–39] A comparison of the theoretical predictions for the low-frequency region with experiment turns out difficult in the absence of INS data due to the weak optical activity of the intercage modes. The range obtained by the first-principles calculations of Adams *et al.* for [2+2] cycloadded neutral $C_{60}$ molecules ($10\ \text{meV} \leqslant \hbar\omega \leqslant 20\ \text{meV}$) agrees well with our INS results on charged chains in $AC_{60}$. A further going comparison is not possible at the present stage as the calculations are limited to the zone center modes while the experimentally determined vibrational density-of-states contains particularly large contributions from the zone boundary modes.

To obtain a better understanding of the low-frequency lattice vibrations we have, therefore, carried out lattice-dynamical calculations for $Rb_1C_{60}$ using a hybrid model which combines force fields and potential-derived atom-atom interactions. In previous studies of the low-frequency part of the lattice dynamics of $C_{60}$ and $A_3C_{60}$ we have adopted an external mode approach.[24] This approximation,

TABLE I. Van der Waals parameters for the different type of bonds. We use a Lennard-Jones parametrization of the form $V(r)=D[(\sigma/r)^{12}-2(\sigma/r)^{6}]$.

| Bond | $\sigma$ (Å) | $D$ (meV) |
|---|---|---|
| C-C | 3.82 | 2.85 |
| Rb-C | 4.42 | 1.3 |
| Rb-Rb | 5.11 | 1.95 |

which treats the $C_{60}$ molecules as rigid bodies and ignores any intramolecular vibrations, works well as long as the frequencies of the external and internal modes are separated by a sufficiently large gap. For the polymer phase, this condition is no longer satisfied. Therefore, in the calculations presented here, all C and Rb atoms are treated as independent dynamical units.

Lattice geometry and orientations of the $C_{60}$ molecules were chosen according to the structural models proposed by Stephens *et al.*[1] (orthorhombic space group $P\,2/m\,2_1/n\,2_1/n$ with two $Rb_1C_{60}$ units in the primitive cell). In addition we acknowledge experimental[1] and theoretical[37] indications of a deformed $C_{60}$ cage. The C atoms participating in the [2+2] cycloaddition are shifted in such a way as to change the bond lengths of this four-C ring to 1.58 and 1.56 Å for the interfullerene and intrafullerene bonds, respectively.

The on-ball C-C interaction is described by a force field proposed by Jishi *et al.*[40] consisting of four longitudinal Born-von-Kármán and four angle-bonding force constants. This model was developed to reproduce all optic active internal modes of the neutral $C_{60}$ molecule and for the present purpose predicts the overall shape and range of the whole intramolecular spectrum sufficiently well. Van der Waals atom-atom potentials are introduced for C-Rb, Rb-Rb bonds as well as for bonds between two C atoms belonging to two different molecules, taking into account all bonds with lengths between 3.1 and 14.0 Å . Table I shows the Lennard-Jones parameters used in all calculations. With respect to our previous model calculations,[24] we have slightly altered two parameters. $D_{C\text{-}C}$ was taken from Ref. 41, which improved the position of the main low-energy libration peak. Furthermore, we slightly enhanced $D_{C\text{-}Rb}$ to shift some Rb weight up to 7 meV simulating the observed shoulder for the polymer phase (see discussion below).

To simulate the proposed [2+2] cycloaddition bond we use a minimal set of three parameters consisting of a bond stretching force constant $F_{\text{inter}}$ for the interfullerene C-C bond and two angle bending force constants: $K_1$ is related to the angle spanned by the interfullerene C-C bond and the (6,6) bond (treated as a single bond in the calculations), $K_2$ to the angles spanned by the interfullerene C-C bond and the (5,6) bonds. The three parameters were varied to optimize the description of the upper frequency part of the external mode spectra (10–25 meV). Neither transverse force constants nor diagonal interactions within the fourfold ring are included in this model.

To estimate the changes in the phonon dynamics induced by the charge transfer from the Rb ions to the $C_{60}$ molecules we have equally carried out calculations including Coulomb forces by assuming an ionic lattice with effective charges of

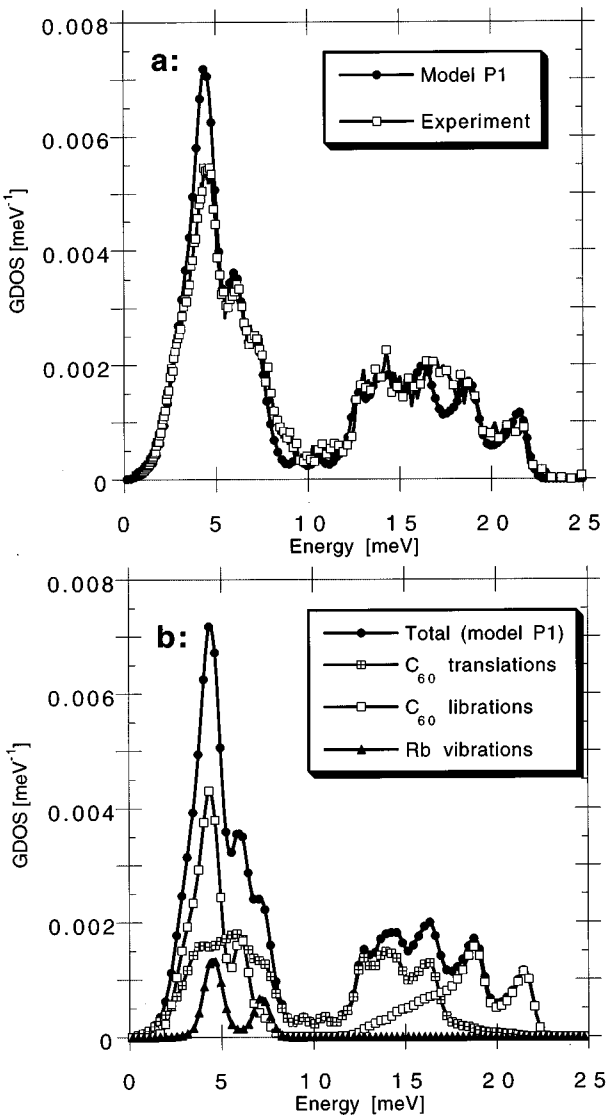


FIG. 4. Model (P1) GDOS (normalized to 1) of external modes for the polymer phase. (a) Comparison with the experimental spectrum. (b) The corresponding decomposition into contributions from $C_{60}$ translations, $C_{60}$ rotations, and Rb vibrations.

$+1e$ on the Rb sites and $-1/60e$ for each C atom. We found, however, that this interaction only produces very small weight shifts in the region around 5 meV, and, therefore, can safely be ignored in our analysis.

When comparing with the experimental data we determine the spectral weight in absolute units by using the first intramolecular peak, corresponding to the fivefold degenerate $H_g(1)$ modes in icosahedral $I_h$ $C_{60}$, as a standard. Despite its simplicity, the model (denoted P1 thereafter) gives a very good description of the experimental GDOS (see Fig. 4). It is particularly satisfying that both the Born von Kármán ($F_{\text{inter}}$) and valence force constants ($K_1$, $K_2$) obtained for the [2+2] intercage coupling (Table II) compare very favorably with the interactions used for the $C_{60}$ pentagons [short (5,6) bonds] thus giving physical weight to the models.

A good understanding of the vibrational spectrum can be obtained from the phonon dispersion, which is shown in Fig. 5 for selected high symmetry directions. An analysis of the characters of the phonon modes involved leads to the following interpretation of the spectrum.

TABLE II. Force constants used in the lattice dynamical model calculations. The angle force constants are defined as $K=1/(r_1 r_2)\partial^2\Phi/\partial\alpha^2$, i.e., as the second derivative of the lattice potential $\Phi$ with respect to the angle $\alpha$, divided by the lengths $r_1$ and $r_2$ of both bonds attached to the angle. They, therefore, possess the same units ($10^3$ dyn/cm) as the longitudinal Born von Karman force constant $F_{\text{inter}}$.

| Model | $F_{\text{inter}}$ | $K_1$ | $K_2$ |
|---|---|---|---|
| P1 [2+2] | 200 | 40 | 30 |
| D1 [2+2] | 100 | 23 | 20 |
| D2 sb | 320 | 60 | 60 |
| D3 sb | 235 | 33 | 29 |

The GDOS in the region 12–25 meV has almost equal contributions from rotational and translational modes. This includes librations around axes perpendicular to the chain direction, which result in shear distortions of the fourfold ring. The translational weight is partly produced by $C_{60}$ displacements along the chain direction. Such modes exhibit very steep dispersions along lines parallel to the $k_x$ direction in reciprocal space, and are also responsible for the filling of the pseudo gap around 10 meV. The second translational contribution comes from modes with $C_{60}$ motions perpendicular to the chains. The broad pseudo gap at 10 meV has its origin in a strong hybridization between these translational branches and the librations mentioned above. Librations around the chain axis are much softer and produce the main peak in the spectrum just below 5 meV. This is of particular interest for the discussion of the low-temperature behavior in Sec. VI. The Rb contribution to the GDOS is fully included in the lower part ($<8$ meV). This agrees with our results on $A_3C_{60}$ which show that the Rb ions occupying octahedral sites are weaker bound.[24] No distinct peaks are observed in the spectra which would scale with $M_{\text{alkali}}^{-0.5}$. There is, however, a shoulder at 7 meV in the GDOS of $Rb_1C_{60}$ not observed in $Cs_1C_{60}$ and $K_1C_{60}$ which we tentatively assign to optical Rb vibrations (see Fig. 4).

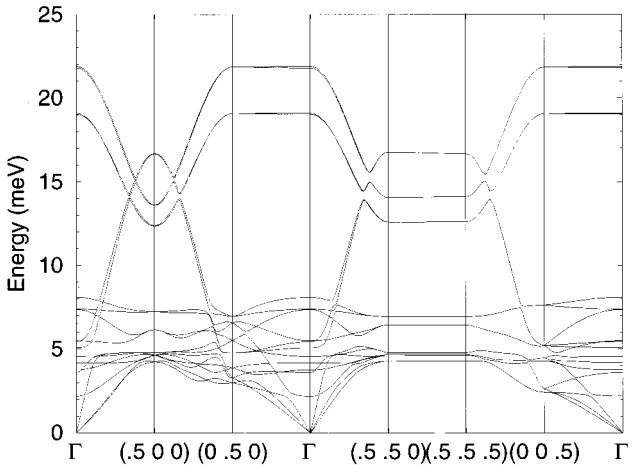


FIG. 5. Dispersion relation of the external modes for the polymer phase as obtained with model P1 described in the text. The two $Rb_1C_{60}$ units in the primitive cell lead to the 18 external dispersion curves shown. The polymer chains are aligned parallel to the orthorhombic $k_x$ direction.

### C. Dimer phase

By quenching the $Rb_1C_{60}$ powder from 450 to 77 K and subsequently heating to 200 K a new phase forms consisting of $(C_{60})_2^{-2}$ dimers. So far it was not possible to refine the positions of the carbon atoms participating in the dimer bond from the powder-diffraction data.[6] However, theoretical calculations[23] and structural investigations[6] agree that most probably the charged dimers are single bonded. As the issue is not completely settled we decided to take an unbiased approach simulating both a [2+2] cycloadded (model D1: monoclinic space group $C2/m$)[4] as well as a single-bonded dimer structure (models D2 and D3: monoclinic space group $P2_1/a$).[6] Model D2 treats the $C_{60}$ molecules as undistorted while for model D3 the intercage nearest-neighbor atoms were displaced along the dumbbell axis to simulate the relaxation of the bonds in the contact region. The intercage bond distance for model D3 was chosen as 1.6 Å, which we consider a physical value in light of the polymer data. The on-ball interactions as well as the interatomic potentials used are identical to the ones of the polymer model.

The crude characterization of the phonon spectra in the dimer phase does not depend on the model chosen (see Fig. 6). Because of the weak coupling of a dimer to its environment, the phonon dispersion features very flat optic branches (see Fig. 7) consisting of intradimer vibrations, which lead to sharp peaks in the GDOS. The two highest of those peaks at 12.2 and 13.0 meV involve both $C_{60}$ librations and translations perpendicular to the dimer axis, whereas antiphase translations parallel to the dimer axis (bond stretching modes) are responsible for the peak at 10.4 meV. The peaks in the lower part of the spectrum arise primarily from librations. The details in this part are less well reproduced by the models. In the case of the [2+2] dimer the model predicts three librational bands at approximately 3, 4, and 5 meV plus a gap at 6 meV, while the experimental data feature only two weak peaks and no gap. For the single bonded dimer the experimental two-peak structure is reflected in the calculations, however, the positions, in particular of the first peak, are underestimated. These discrepancies should not be overinterpreted given the simplicity of our models. In particular, they do not allow us to disciminate among the two bonding scenarii. The Lennard-Jones potentials have been optimized for pristine $C_{60}$. It, therefore, comes as no surprise that the first librational peak for the single-bonded dimer comes to lie at 2 meV. The relative size of the weights in the lower and upper part of the spectrum agrees well with experiment. For example, D1 predicts that 77% of the external GDOS is contained below $<9$ meV as compared to 73% estimated from the data. A particular feature of the experimental dimer spectrum is the strongly enhanced intensity between 1 and 2 meV leading to a nearly linear increase of the experimental density-of-states in that region. It is difficult to conceive a way of modifying our model to reproduce this enhancement, as the slope of the accoustic branches is basically determined by the Van der Waals interactions. The enhancement is specific to the dimer, i.e., it disappears upon transformation to the polymer (see Sec. V B). A possible explanation for this feature is orientational or bonding disorder (boson peak) which would also offer an explanation for the difficulty of the models to describe the low-lying librational branches.

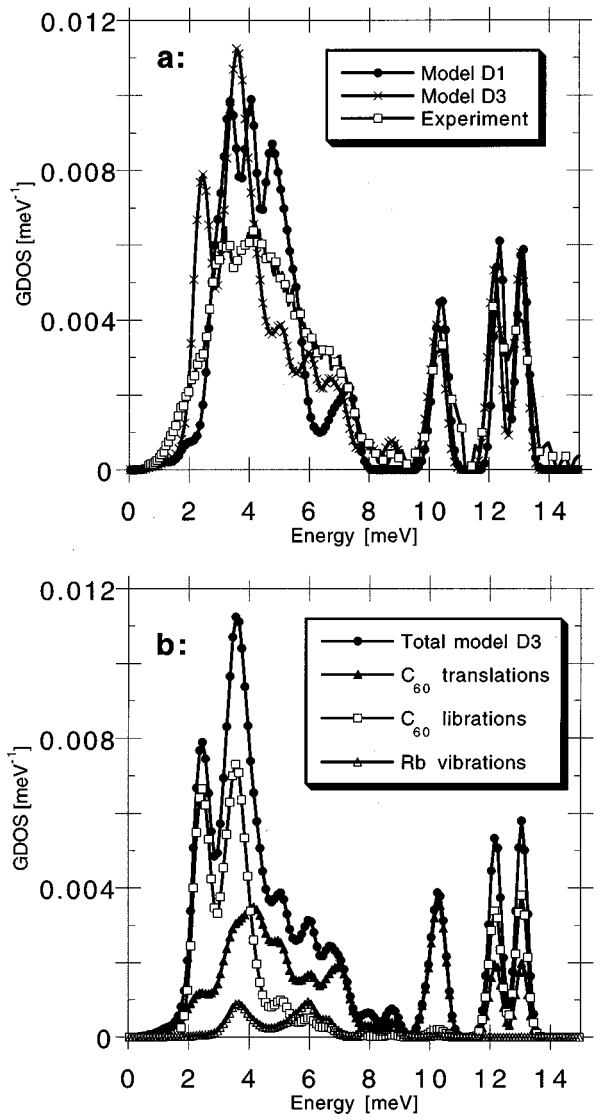


FIG. 6. GDOS of external modes for the dimer phase. (a) Comparison of models D1 and D3 with the experimental data. (b) Decomposition as in Fig. 4(b) using model D3.

Structural investigations[6] show, on the other hand, no clear indications for orientational disorder.

Although leading to a similar quality of data description the models differ in their physical interpretation. Within the [2+2] bonding scenario the coupling of $C_{60}$ molecules turns out significantly weaker in the dimer than one would have expected from the polymer. The stretching force constant $F_{\text{inter}} = 100\,000$ dyn/cm for the single bonds is roughly three times smaller than the one found within graphite planes and two times smaller than the one used to describe the short (5,6) on-ball bonds. In the case of neutral molecules this finding could be used as a strong argument to refute [2+2] bonding in the dimer. For anions one has to be more careful as the symmetry requirements encountered by the donated electrons are completely different for $(C_{60})_2^{-2}$ and $(C_{60})_n^{-n}$. While in the polymer there is a one-to-one correspondence between the number of donated electrons and the number of intercage bonds there are two donated electrons per intercage bond in the dimer. These differences may result both in longer bond distances and weaker couplings. Given

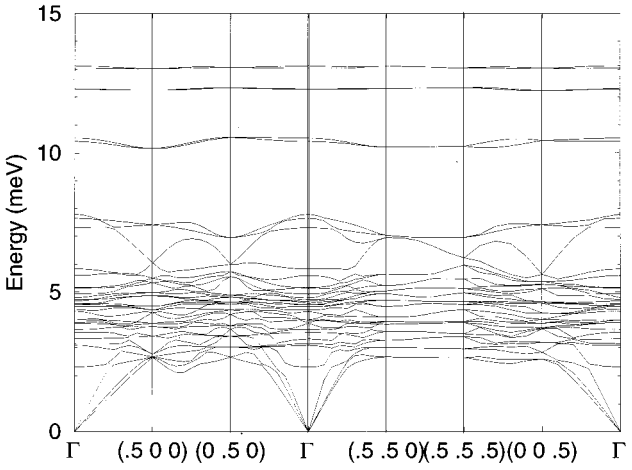


FIG. 7. Dispersion relation of the external modes for the dimer phase as obtained with model D1. The four $Rb_1C_{60}$ units in the primitive cell leading to 36 external dispersion curves. The acoustic spectrum is significantly softer than in the polymer as expected for a molecular system $[(C_{60})_2^{-2}]$ bound by Van der Waals forces.

the weak couplings found for the [2+2] bond the difficulties of model D2 (undistorted single-bonded dumbells) to reproduce the position of the bond-stretching peak at 10.2 meV, and this despite the already large value of $F_{\text{inter}}$, comes as a surprise. Deeper analysis reveals that the origin for this shortcoming is to be found in the radial softness of the contact regions. Moving the contact atom radially out appreciably stiffens this region and $F_{\text{inter}}$ drops to the (5,6) bond value of 235 000 dyn/cm (model D3). This result demonstrates the influence of the unfortunately unknown relaxed atom positions on the model parameters.

The valence force constants are physically reasonable for all three models, provided one corrects for the varying bond lengths. In particular for model D3 they can practically be transferred from the on-ball pentagon interactions.

Summarizing we find that while unable to discriminate the two bonding senarii by the quality of the data reproduction the interpretation of the coupling parameters favors single bonded dimers.

## IV. INTERNAL MODE SPECTRUM

The fact that the evolution of the internal and external modes can be observed simultaneously under exactly the same experimental conditions is an invaluable advantage of INS for the study of the phase transitions. In Fig. 8 we show a comparision of the density-of-states in the region 25 meV $< \hbar\omega <$ 55 meV between pristine $C_{60}$, $Rb_1C_{60}$ both in the fcc rotator phase, $Rb_3C_{60}$ in the fcc merohedrally disordered phase, and $Rb_6C_{60}$ in the bcc ordered phase. The data have been obtained in down scattering with the instrument DN6 using an incident energy of 70 meV. The fcc signals are broadened due to the rotational diffusion of the cages. If we neglect the crystal field perturbations caused by the presence of the Rb ions then the differences observed between pristine $C_{60}$ and $Rb_1C_{60}$ must be due to charge transfer.[42] In the region investigated only the band corresponding to the $H_g(2)$ modes in pristine $C_{60}$ reacts visably (see arrow in Fig. 8). This reaction is, however, weak when compared with the

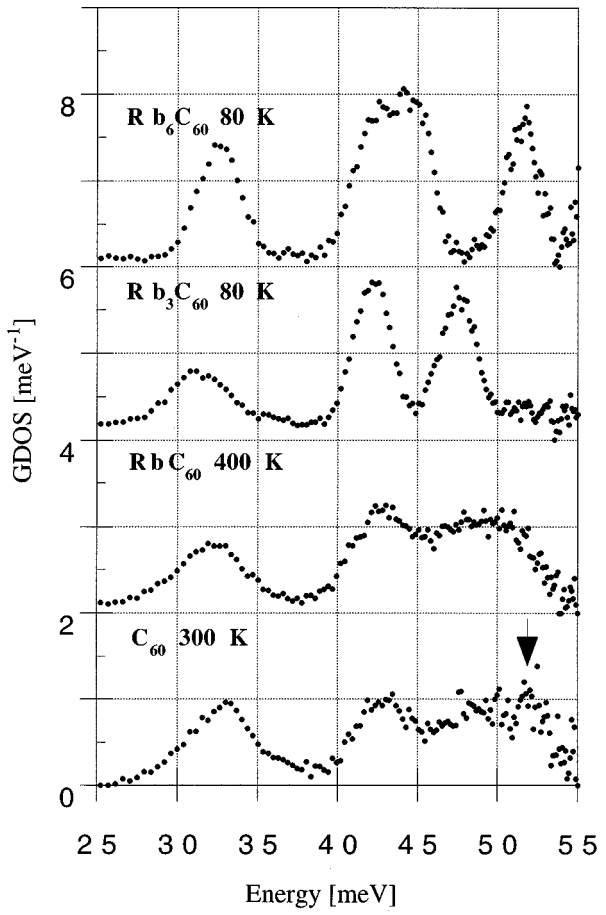


FIG. 8. Generalized density-of-states (normalized to $3n=183$) in the lower internal mode region. Shown are $Rb_1C_{60}$ and pristine $C_{60}$ both in the fcc (rotator), $Rb_3C_{60}$ in the merohedrally disordered fcc, and $Rb_6C_{60}$ in the bcc ordered phase. The relative $y$ axes have been shifted by $2\text{meV}^{-1}$. The positon of the $H_g(2)$ mode in pure $C_{60}$ is indicated by the arrow. No corresponding peak is observed in $Rb_1C_{60}$.

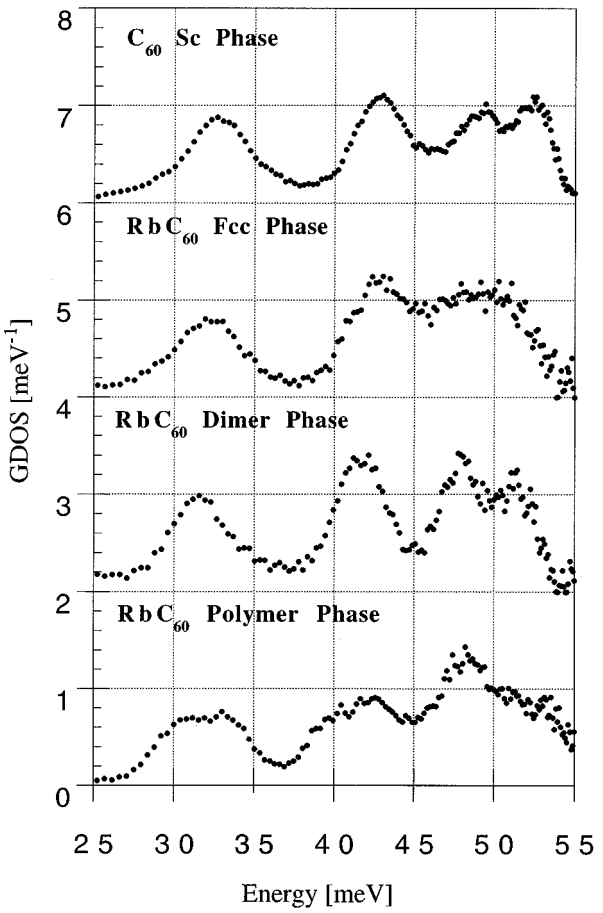


FIG. 9. Generalized density-of-states in the lower internal mode region for pristine $C_{60}$ in the ordered sc phase and comparision with $Rb_1C_{60}$ in the plastic, polymer, and dimer phases. The relative $y$ axes have been shifted by 2 $\text{meV}^{-1}$.

dramatic redistribution of internal mode intensities taking place both in the metallic $Rb_3C_{60}$ and insulating $Rb_6C_{60}$ compounds. No temperature variations of the GDOS are observed down to 80 K in any of the compounds. If we interpret the reaction of the GDOS to charge transfer as a sign of on-ball electron-phonon coupling then this coupling is rather weak in the singly charged cages, at least in the range of energies investigated here.

Figure 9 illustrates the changes in the internal mode spectra linked to the solid-state chemical reactions. Shown are pristine $C_{60}$ in the ordered sc phases as well as $Rb_1C_{60}$ in the fcc, polymer and dimer phase. The internal modes clearly reflect the deformation of the cages. This is best demonstrated by the splitting of the $I_h$ $C_{60}$ $H_g(1)$ mode at 33 meV into two parts centered at 29 and 33 meV in the polymer phase of $Rb_1C_{60}$. The splitting is absent in the experimental fcc and dimer spectra confirming early Raman experiments.[20] More generally it can be stated that, apart from some general softening, the dimer spectrum of $Rb_1C_{60}$ obtained by INS in the range from 25 to 55 meV strongly resembles the spectrum of pristine $C_{60}$ in the orientationally ordered simple cubic phase, while an appreciable redistribution of intensities is observed for the polymer phase. By checking the $Q$ dependence of the inelastic signals we can estimate the energy range over which such a redistribution takes place. This is demonstrated in Fig. 10 for the $H_g(1)$ region. The well-structured $Q$ dependence of the signals integrated over the range from 28 to 36 meV in poly-

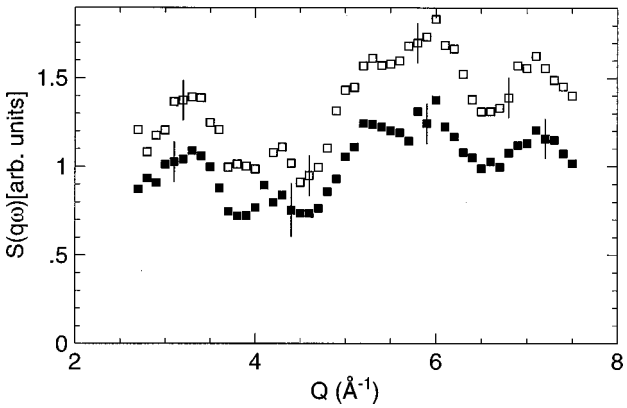


FIG. 10. $Q$ dependence of the scattering function of $Rb_1C_{60}$ (full squares) in the polymer phase at 300 K integrated over the band from 28 to 36 meV and comparison with pristine $C_{60}$ (open squares) at 240 K. The units are arbitrary and no corrections for Debye-Waller factor and varying sample quantities have been applied.

meric $Rb_1C_{60}$ is strikingly similar to the one observed for pristine $C_{60}$, indicating that the character of the modes in this band is preserved. This holds equally well for the bands 36–44 meV, 44–50 meV, and 50–55 meV. In addition, the experimental $Q$ dependences agree well with the predictions of the lattice dynamical model.

Concerning the origin of the $H_g(1)$ splitting one might think it related to stronger cage deformations induced by the [2+2] bonding in the polymer. The lattice dynamical models show that this is not a necessary condition. The splitting is well reproduced by the polymer model P1 and absent in all the dimer models D1–D3, i.e., independent of the type of bonding or the degree of deformation assumed. We therefore, conjecture that the splitting arises from the dispersion introduced in the $H_g(1)$ modes by the polymerization, whereas in the case of the dimer the modes stay Einstein-like.

## V. STRUCTURAL PHASE TRANSITIONS

### A. fcc ↔ polymer transition

In order to investigate the dynamical changes related to the fcc ↔ polymer transition we have carried out several series of measurements in the temperature range from 300 to 430 K. The intensity distribution in the region from 10 to 25 meV is specific to the polymer chains and can, therefore, be used to monitor the number of monomers bound in polymers within the sample. Upon cooling (Fig. 11) we find that the gap intensities build up rather abruptly and later evolve slowly. The same holds for the low-frequency part, where we witness a rather abrupt loss of quasielastic intensity below 400 K. The susceptibilities relax afterwards visibly over several hours and down to 330 K. Thermal equilibrium is certainly not achieved for the 360 K measurement as clearly evidenced by the inversion $\omega^{-1}\chi''[\omega](360\ \mathrm{K}) > \omega^{-1}\chi''[\omega](370\ \mathrm{K})$ for $\hbar\omega < 5$ meV. The 360 K run preceded the 370 K run thus leaving the system less time to evolve. The spectral changes encountered upon cooling are qualitatively undistinguishable from the ones registered upon heating the fully equilibrated samples besides a general hysteresis (see Table III). Upon heating the changes set in around 350 K, i.e., far below the transition temperature towards the stable fcc phase.

It is tempting to investigate the possibility of expressing the spectra obtained at intermediate stages of the polymerization process as superpositions of the inital (rotator) and final (equilibrated polymer) functions. In Fig. 12 we show the difference spectra of the generalized susceptibilities $\omega^{-1}\chi''[\omega]$ for $Rb_1C_{60}$ as obtained by subtracting the lowest temperature results and after scaling to a common area in the inelastic range from $-4 < \hbar\omega < 2$ meV. Please note that due to the scaling the relative errors for the lower temperatures shown are relatively high. As can be seen, all curves, inclusive of the one obtained for the 430 K rotator phase, coincide within the experimental uncertainties. This observation holds both in the low-frequency quasielastic region and in the gap region. The asymmetry of the quasielastic signal (see Sec. III A) arises from the $Q$ integration, which covers inequivalent regions on the down- and up-scattering side. The validity of the superpositon principle constitutes clear evidence for the presence of more or less extended monomer clusters within the polymer matrix if one considers the following facts: (i) the contributions to the susceptibilities from ideal harmonic vibrations are independent of temperature, (ii) the line shape of the quasielastic signal is basically determined by the weakly $T$-dependent $D_r$ (see Sec. III A), while (iii) the intensities scale weakly with $T^{-1}$.

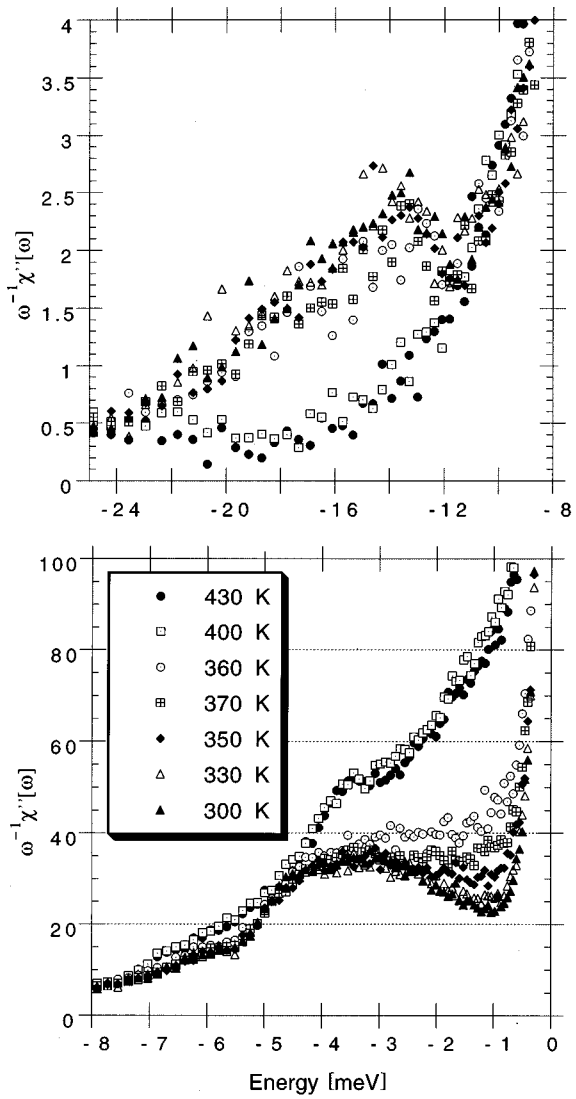


FIG. 11. Temperature evolution of the generalized susceptibility $\omega^{-1}\chi''[\omega]$ for $Rb_1C_{60}$ in the polymer phase ($T<400$ K) upon cooling and comparison with the plastic phase ($T>400$ K). The successive measurements interrupted by short cooling intervals were taken in the order 430 K (45 min), 400 K (60 min), 360 K (30 min), 370 K (60 min), 350 K (60 min), 330 K (60 min), and 300 K (60 min). The thermal history is important for the interpretation of the data because the polymerization rate is temperature dependent.

From the scaling factors of the quasielastic intensities we determine the percentage of monomers present in the system as a function of time and temperature. The result is summarized in Table III after correction for the $T^{-1}$ dependence discussed above. It is, on the other hand, impossible to predict the size of the monomer regions from the inelastic data beyond the fact that isolated monomers are incompatible with the observation that the differences in Fig. 12 scale over the complete low-frequency spectrum including the collective translational excitations.

TABLE III. Amount of monomers present in the mixed phase. For the cooling sequence we indicate in addition to the temperature the mean time elapsed between the 400 K measurement and the data acquisition. The 300 (cooling) and 320 K (heating) spectra are taken as the respective reference points, i.e., they correspond to zero percent monomers. Errors are of the order of 20%.

| Temperature [K] | Time elapsed [min] | Fraction of monomers |
|---|---|---|
| 360 (cooling) | 15 | 0.29 |
| 370 (cooling) | 60 | 0.15 |
| 350 (cooling) | 120 | 0.07 |
| 330 (cooling) | 180 | 0.02 |
| 350 (heating) | | 0.02 |
| 370 (heating) | | 0.09 |
| 385 (heating) | | 0.21 |

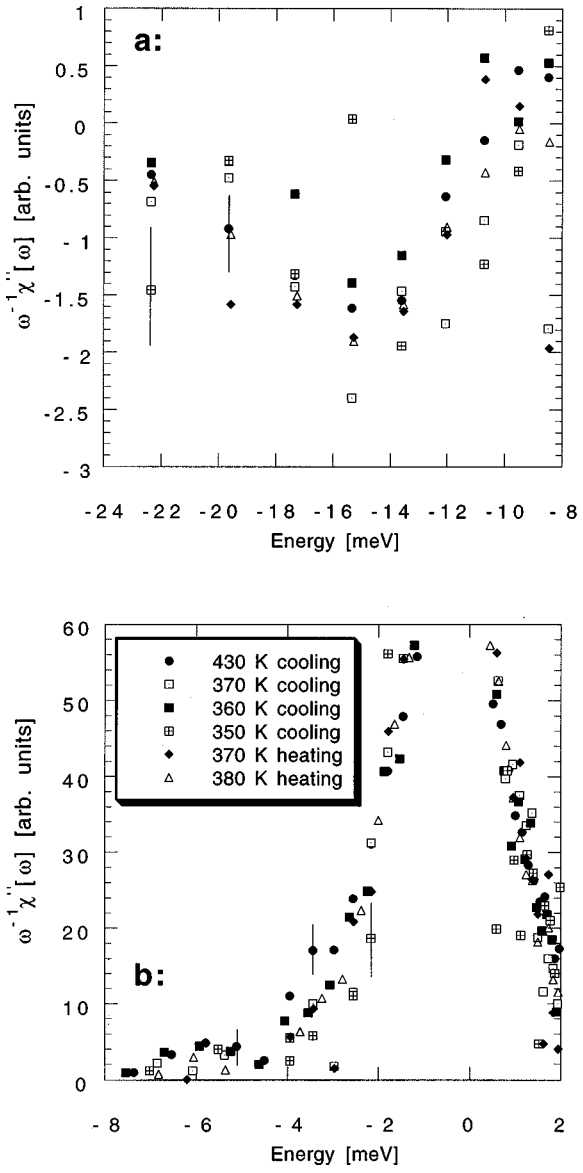


FIG. 12. Difference INS spectra of the generalized susceptibility $\omega^{-1}\chi''[\omega]$ for $Rb_1C_{60}$ as obtained by subtracting the 320 K result. Normalization was carried out by scaling to a common area in the range $-4$ meV $<\hbar\omega<2$ meV.

In summary, we find that the polymer phase of $Rb_1C_{60}$ becomes unstable at about 350 K making way for a heterogeneous phase consisting of monomer clusters embedded in a polymer matrix. We are, therefore, not dealing with a simple fcc $\leftrightarrow$ polymer first order transition. The monomer content changes smoothly with temperature and can be described by an effective activation energy of about $700\pm100$ meV. Up to at least 395 K this heterogeneous phase shows no signs of instability over several hours. It features more than 40% of monomers before it finally around 400 K converts with a strongly $T$-dependent rate into the isotropic monomer phase. The onset of excess intensities upon heating correlates exactly with the observation of endothermal signals in the differential scanning calorimetry (DSC) measurements.[43] The DSC results are, on the other hand, confirmed by Monte Carlo-type calculations[35] which based on known values of activation energies predict the presence of monomers. Between 300 and 350 K the spectrum behaves harmonically. This contrasts sharply with the strong softening of the libronic modes observed in $A_3C_{60}$ compounds[47] and implies that the breakup of the polymer bonds is not preceded by an important buildup of large-amplitude motions of the cages. Upon cooling the system takes a long time to reach equilibrium. More experiments are under way to determine the $T$ dependence of the conversion rates. The polymer content slowly increases at the expense of the monomer clusters. For example, after 15 min at 360 K close to 30% of the cages are still not bound to polymers.

It is interesting to note that the changes in the dynamics observed here resemble in many aspects the ones found in glass-forming polymers.[44] As in our case the changes have their origin in the heterogeneity one may ask the same question for the glass formers.

### B. Dimer → polymer transition

The metastable dimer phase of $Rb_1C_{60}$ evolves gradually into the polymer phase. The rate of conversion is highly temperature dependent as already known from infrared reflectivity[45] and DSC measurements.[43] Below 240 K this process is too slow and above 280 K too fast to be observed on the time scale of our INS experiments. In Fig. 13 we show the time evolution of the generalized susceptibility $\omega^{-1}\chi''[\omega]$ of the quenched sample at 260 K. Each of the six curves corresponds to 3 h of measuring time. We have chosen to decompose the spectrum into three parts which represent the different energy scales present in the system. The thermal history of the sample was as follows: quench from 430 to 77 K, 6 h measurement at 90 K, fast heating (30 min) to 250 K, 9 h measurement, fast heating to 260 K, 18 h measurement. Contrary to what is claimed by Kosaka *et al.*[46] our system was not in a metastable sc phase directly after the quench but right from the start showed the inelastic spectrum of the dimer phase.

In the region 8 meV $<\hbar\omega<25$ meV the spectrum constitutes a convenient measure of the quantity of cages bound either in dimers or polymers. The amount of dimers had already slightly decreased at the beginning of the 260 K measurement. As time passes the dimer peaks continuously become weaker. Remnants of the peaks can still be observed after 15 h. The loss of the typical dimer intensities is accom-

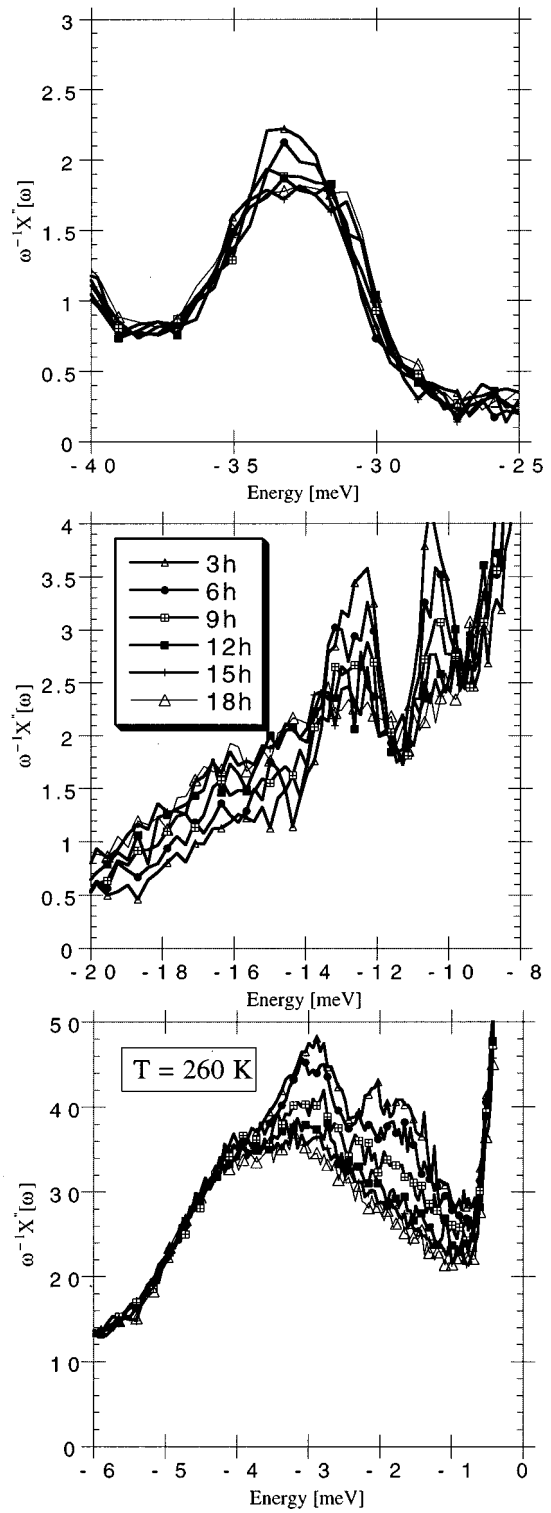


FIG. 13. Time evolution of the generalized susceptibility $\omega^{-1}\chi''[\omega]$ for the quenched $Rb_1C_{60}$ sample at 260 K. Each curve corresponds to 3 h of measuring time.

panied by a buildup of intensities in the polymer region (12 meV$<\hbar\omega<$25 meV). However, not only the integrated intensity but also the line shape of this buildup changes with time.

The evolution of the low-frequency spectrum ($\hbar\omega<8$ meV) happens in two steps. During the first 9 h the structures at 2 and 3 meV disappear leaving a broad distribution which qualitatively already resembles the final polymer spectrum. This distribution then slowly relaxes.

In the case of the first internal modes $[H_g(1)]$ the main variations happen during the first 9 h and thus correlate with the changes in the low-frequency region. Due to the poorer resolution in the case of this experiment as compared to the previous one the splitting of the $H_g(1)$ modes shown in Fig. 9 for the polymer phase reduces to a broadening.

The following conclusions can be drawn. As the intermediate spectra cannot be expressed as a superposition of the initial (dimer) and final (polymer) states a dimer $\rightarrow$ polymer transition via the growth of polymer domains must be ruled out. Therefore, at those stages the system must either be in a microscopically disordered state and/or a third phase must come into play. The continuous line-shape change observed in the gap region clearly favors microscopic disorder linked to a statistical chain length distribution $p(n)$ which evolves gradually with time. For example, more than 50% of the cages have become part of polymers after 9 h. This seems to constitute a threshold beyond which we lose most of the dimer signatures in the low-frequency ($\hbar\omega<8$ meV) and internal mode spectrum. As we are dealing with very slow evolutions the disordered intermediate systems can be frozen into glassy states by quenching the samples to low temperatures.

The existence of transient cubic monomer phases during the transformation process is claimed by several authors.[4,43,46] This question is of great importance for the understanding of the polymer formation. On one hand, freely rotating monomers should speed up the polymer formation by producing correct alignments of bonds on adjacent cages with a high probability. On the other hand, polymer growth from a cubic monomer phase bears the possibility of large geometrical frustrations which may hinder a complete polymerization. As the pseudo-orthorhombic dimer phase already features a preferred direction geometrical frustrations would play a minor role for direct chain nucleation. In the inelastic spectra at 260 K we observe, at no time, strongly enhanced signals below 2 meV which would indicate fast reorientations of monomer cages. Therefore, if the polymer formation process includes the breakup of dimers into monomers, these monomers are either not rapidly reorienting or, if rapidly reorienting, on the time scale of the complete transformation process instantaneously rebound into polymers. In the case of dimers bound by single bonds such a breakup into monomers becomes a precondition for polymerization due to the fact that the singly bound dimers cannot enter another bonding.

## VI. LOW-TEMPERATURE REGION

As already outlined in the Introduction $AC_{60}$ compounds show appreciable changes in their electronic properties at low temperatures. We have, therefore, extended the INS experiments on the instrument IN6 down to 45 K. For still lower temperatures the signal-to-noise ratio is insufficient to obtain reliable information in the frequency region of interest.

In Fig. 14(a) we show the temperature evolution of $\omega^{-1}\chi''[\omega]$ for the polymer state of $Rb_1C_{60}$. There is a remarkable, continuous buildup of intensity in the region 1.5

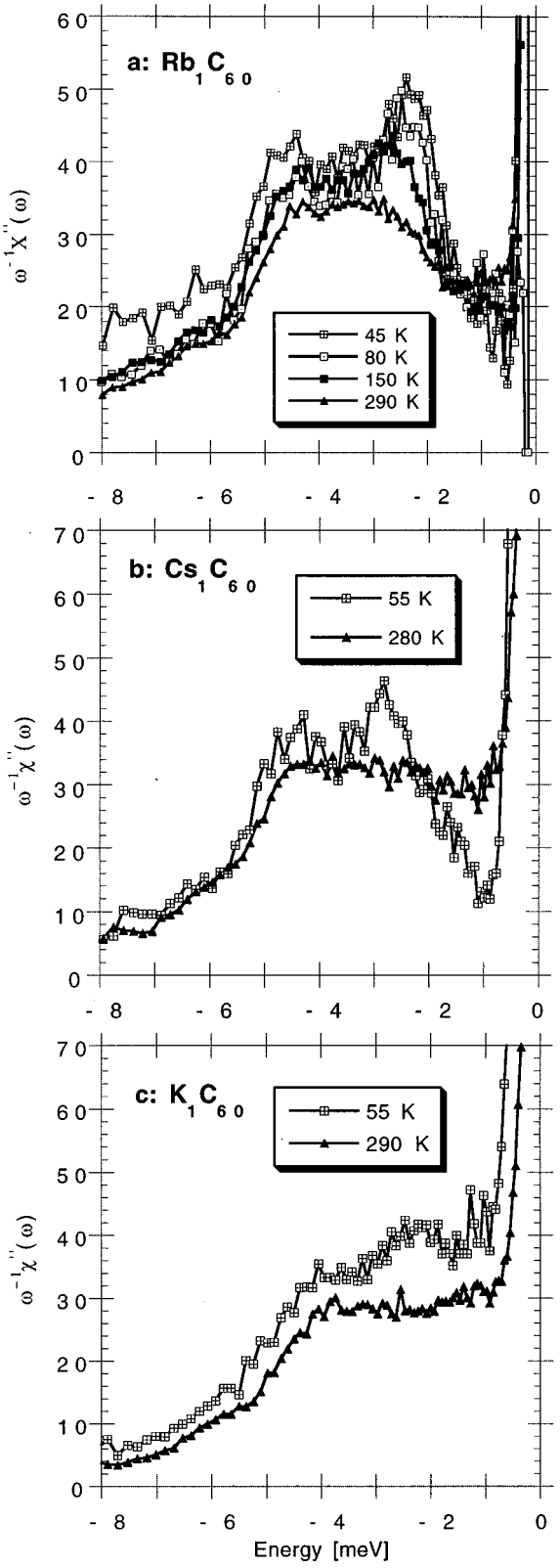


FIG. 14. Evolution of $\omega^{-1}\chi''[\omega]$ for the polymer state of $Rb_1C_{60}$ in the low-temperature region (a) and comparision with $Cs_1C_{60}$ (b) and $K_1C_{60}$ (c).

meV$<\hbar\omega<$3 meV when going from 300 to 80 K. This buildup is completely reversible and within the data statistics does not continue to still lower temperatures (i.e., upon approaching the MIT transition). When expressed as a density-of-states the $T$-dependent buildup of intensity in $\omega^{-1}\chi''[\omega]$ leads to a softening of the excitation spectrum. The $Q$ dependence of the intensities in question is very similar to the one calculated[28] for transverse acoustic phonon branches in pristine $C_{60}$.

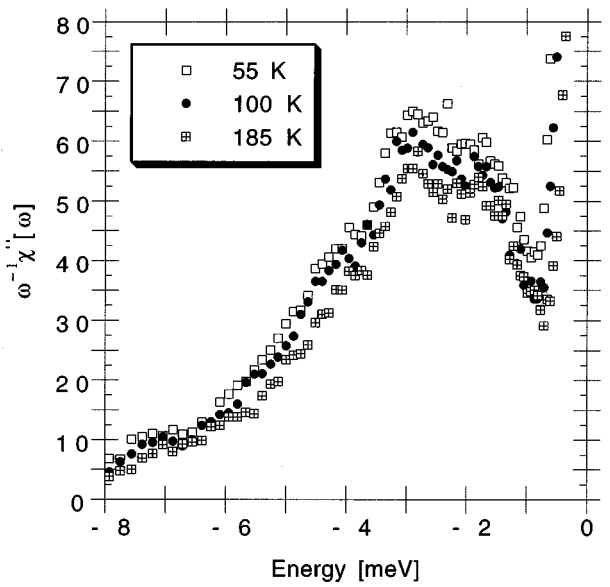


FIG. 15. Temperature evolution of $\omega^{-1}\chi''[\omega]$ for the dimer state of $Rb_1C_{60}$ in the low-temperature region.

To gain additional insight into the mechanism responsible for the softening we have carried out low-temperature measurements at 55 K for the dimer state of $Rb_1C_{60}$ as well as for the polymer states of $K_1C_{60}$ and $Cs_1C_{60}$. Concerning the dimer state, we merely observe a general increase of $\omega^{-1}\chi''[\omega]$ when going from 200 to 55 K (see Fig. 15). This increase of about 10% can be explained by the $T$ dependence of the Debye-Waller factor. No redistribution of intensities is observed in $G(\omega)$. At 300 K the inelastic spectra of polymerized $K_1C_{60}$ and $Cs_1C_{60}$ are very similar to the one of $Rb_1C_{60}$. Significant differences can only be observed in the acoustic region. Subtracting the $Rb_1C_{60}$ spectrum from the $Cs_1C_{60}$ spectrum we end up with a difference spectrum containing quasielastic contributions similar to the ones shown in Fig. 12. We take this as an indication for small amounts of monomers frozen into the $Cs_1C_{60}$ polymer sample. The difference spectrum of $K_1C_{60}$, on the other hand, is truly inelastic, a feature which can be explained by an admixture of the stable $K_3C_{60}/C_{60}$ phase. Upon cooling $\omega^{-1}\chi''[\omega]$ changes: strong in $Rb_1C_{60}$, somewhat weaker in $Cs_1C_{60}$ and practically not in $K_1C_{60}$. The strength of the nonharmonic behavior, therefore, correlates with the transition temperature for the MIT ($T_c\approx$50 K for $Rb_1C_{60}$, $T_c\approx$ 40 K for $Cs_1C_{60}$, no transition in $K_1C_{60}$).

The low-temperature softening is in many respects, including the $Q$ dependence, reminiscent of a softening observed in superconducting $A_3C_{60}$ compounds.[47] The fact that no anomalous behavior can be detected in the insulating phases ($Rb_6C_{60}$ and $Rb_1C_{60}$ in the dimer state) strongly indicates that it is related to electron-phonon coupling in the metallic state. Although this line of argument is plausible, one has to discuss the possibility that structural disorder and its gradual freezing out produce similar effects. While the

insulating $Rb_6C_{60}$ is orientationally ordered[48] the superconducting compounds show merohedral disorder.[49] To our knowledge, so far no reliable information exists concerning the orientational ordering in polymeric or dimer $A_1C_{60}$ compounds. As theoretical calculations show[28,41] orientational disorder leads to a softening of the excitation spectrum. In order to explain the experimental observations disorder would be required to increase upon lowering the temperature, a very unlikely scenario.

If electron-phonon coupling is responsible for the observed gradual softening in the acoustic region changes in the inelastic part of the spectra are to be expected in the vicinity of the metal-to-insulator transition due to the drop in the concentration of conduction electrons. It may be difficult to observe this experimentally as the transition seems to be smeared out over a rather large $T$ range.

## VII. CONCLUSION

We have presented detailed information about the dynamics of $AC_{60}$ compounds obtained by inelastic neutron scattering. The fcc phase is well described by a rotational diffusion model. Lattice dynamical model calculations give a good account of the low-frequency part of the spectra in the polymer and dimer states. They confirm the formation of strong covalent bonds between the $C_{60}$ units. The associated force constants are nearly identical to the ones connected to the short on-ball bonds under the condition that the polymer is [2+2] and the dimer single bonded. The internal mode spectra equally reflect the intercage bonding and show only a weak reaction towards charge transfer.

The very specific fingerprints left by the solid state reactions allow us to follow the phase transitions in real time. During the fcc $\leftrightarrow$ polymer transition we observe the presence of plastic monomer clusters embedded in a polymer matrix. Due to the finite conversion rates the monomer content is a function of both time and temperature and can be quantitatively estimated from the spectra. The dimer $\rightarrow$ polymer transition turns out to proceed via highly disordered intermediate stages.

The spectra of the polymer phase at low temperature show changes going beyond the harmonic crystal approximation which we interpret as signs of electron-phonon coupling. If this coupling plays a role in the MIT transition then from the present result a sharp transition leading to a 3D ordered ground state has to be excluded.

## ACKNOWLEDGMENT

We would like to thank Professor E. W. Fischer for fruitful discussions and S. Jenkins for technical assistance.

[1] P. W. Stephens, G. Bortel, G. Faigel, M. Tegze, A. Jánossy, S. Pekker, G. Oszlányi, and L. Forró, Nature (London) **370**, 636 (1994).

[2] S. Pekker, L. Forró, L. Mihály, and A. Jánossy, Solid State Commun. **90**, 349 (1994).

[3] Q. Zhu, D. E. Cox, and J. E. Fischer, Phys. Rev. B **51**, 3966 (1995).

[4] G. Oszlányi, G. Bortel, G. Faigel, M. Tegze, L. Gránásy, S. Pekker, P. W. Stephens, G. Bendele, R. Dinnebier, G. Mihály, A. Jánossy, O. Chauvet, and L. Forró, Phys. Rev. B **51**, 12 228 (1995).

[5] G. Faigel, G. Bortel, M. Tegze, L. Gránásy, S. Pekker, G. Oszlányi, O. Chauvet, G. Baumgartner, L. Forró, P. W. Stephens, G. Mihály, and A. Jánossy, Phys. Rev. B **52**, 3199 (1995).

[6] G. Oszlányi, G. Bortel, G. Faigel, L. Gránásy, G. M. Bendele, P. W. Stephens, and L. Forró, Phys. Rev. B **54**, 11 849 (1996).

[7] N. G. Chopra, J. Hone, and A. Zettl, Phys. Rev. B **53**, 8155 (1996).

[8] F. Bommeli, L. Degiorgi, P. Wachter, Ö. Legeza, A. Jánossy, G. Oszlányi, O. Chauvet, and L. Forró, Phys. Rev. B **51**, 14 794 (1995).

[9] R. Tycko, G. Dabbagh, D. W. Murphy, Q. Zhu, and J. E. Fischer, Phys. Rev. B **48**, 9097 (1993).

[10] H. Alloul, V. Brouet, E. Lafontaine, L. Malier, and L. Forro, Phys. Rev. Lett. **76**, 2922 (1996).

[11] J. Hone, M. S. Fuhrer, K. Khazeni, and A. Zettl, Phys. Rev. B **52**, 8700 (1995).

[12] S. C. Erwin, G. V. Krishna, and E. J. Mele, Phys. Rev. B **51**, 7345 (1995).

[13] K. Harigaya, Phys. Rev. B **52**, 7968 (1995).

[14] Y. J. Uemura, K. Kojima, G. M. Luke, W. D. Wu, G. Oszlányi, O. Chauvet, and L. Forró, Phys. Rev. B **52**, 6991 (1995).

[15] W. A. MacFarlane, R. F. Kiefl, S. Dunsiger, J. E. Sonier, and J. E. Fischer, Phys. Rev. B **52**, 6995 (1995).

[16] L. Cristofolini, A. Lappas, K. Vavekis, K. Prassides, R. DeRenzi, M. Ricco, A. Schenck, A. Amato, F. N. Gygax, M. Kosaka, and K. Tanigaki, J. Phys. Condens. Matter **7**, L567 (1995).

[17] B. Renker, H. Schober, F. Gompf, R. Heid, and E. Ressouche, Phys. Rev. B **53**, 14 701 (1996).

[18] V. Brouet, H. Alloul, Y. Yoshinari, and L. Forro, Phys. Rev. Lett. **76**, 3638 (1996).

[19] J. Winter and H. Kuzmany, Phys. Rev. B **52**, 7115 (1995).

[20] M. C. Martin, D. Koller, A. Rosenberg, C. Kendziora, and L. Mihaly, Phys. Rev. B **51**, 3210 (1995).

[21] A. M. Rao, Z. Ping, W. Kai-An, G. T. Hager, J. M. Holden, Y. Wang, W. -T. Lee, B. Xiang-Xin, P. C. Eklund, D. S. Cornett, M. A. Duncan, and I. J. Amster, Science **259**, 955 (1993).

[22] Y. Iwasa, T. Arima, R. M. Fleming, T. Siegrist, O. Zhou, R. C. Haddon, L. J. Rothberg, K. B. Lyons, H. L. Carter, A. F. Hebard, R. Tycko, G. Dabbagh, J. J. Krajewski, G. A. Thomas, and T. Yagi, Science **264**, 1570 (1994).

[23] J. Kürti and K. Németh, Chem. Phys. Lett. **256**, 119 (1996).

[24] B. Renker, F. Gompf, H. Schober, P. Adelmann, H. J. Bornemann, and R. Heid, Z. Phys. B **92**, 451 (1993).

[25] B. Renker, F. Gompf, R. Heid, P. Adelmann, A. Heiming, W. Reichardt, G. Roth, H. Schober, and H. Rietschel, Z. Phys. B **90**, 325 (1993).

[26] S. W. Lovesey, *Theory of Neutron Scattering from Condensed Matter* (Oxford Science Publishers, Oxford, 1984), Vol. 1, p. 121.

[27] M. M. Bredov, B. A. Kotov, N. M. Okuneva, V. S. Oskotskii, and A. L. Shak-Budagov, Sov. Phys. Solid State **9**, 214 (1967).

[28] L. Pintschovious and S. L. Chaplot, Z. Phys. B **98**, 527 (1995).

[29] D. A. Neumann, J. R. D. Copley, R. L. Cappelletti, W. A. Kamitakahara, R. M. Lindstrom, K. M. Creegan, D. M. Cox, W. J. Romanow, N. Coustel, J. P. McCauley, Jr., N. C. Maliszewskyj, J. E. Fischer, and A. B. SmithIII, Phys. Rev. Lett. **67**, 3808 (1991); J. R. D. Copley, W. I. F. David, and D. A. Neumann, Neutron News **4**, 20 (1993).

[30] This is confirmed by our IN6 experiments on pristine $C_{60}$. There the first libronic peak is found at 2 meV. The corresponding $Q$ range does not include the first peak in the libronic form factor and the librational degrees of freedom are, therefore, not fully represented in $G(\omega)$.

[31] J. Wuttke, M. Kiebel, E. Bartsch, F. Fujara, W. Petry, and H. Sillescu, Z. Phys. B **91**, 357 (1993).

[32] L. Pintschovius, S. L. Chaplot, G. Roth, and G. Heger, Phys. Rev. Lett. **75**, 2843 (1995).

[33] Short-range orientational order in fcc $C_{60}$ at low temperatures may also be responsible for the observed dependence of the rotational diffusion constant upon temperature, leading to an activation energy of about 35 meV. This value is small if compared to the one obtained by NMR (Ref. 50) (700 K), but in good agreement with three-axis INS data taken at 500 K (Ref. 29). As the NMR data were taken over a different temperature range (up to 340 K), they may find a higher activation energy due to remnants of short-range orientational order.

[34] The above argument would even hold, if the rotational diffusion constants of the two compounds were slightly different, as continuous isotropic rotational movements do not contribute towards a temperature dependence of the elastic intensities. This is due to the fact that there are no preferred molecular orientations in the ideal scenario. When calculating the elastic intensity the molecule can, therefore, be replaced by an isotropic distribution of scattering length, which is tantamount to using a temperature-independent form factor.

[35] T. Pusztai, G. Faigel, L. Gránásy, M. Tegze, and S. Pekker, *Physics and Chemistry of Fullerenes and Derivatives*, edited by H. Kuzmany, J. Fink, M. Mehring, and S. Roth. (World Scientific, Signapore, 1995), p. 302; T. Pusztai, G. Faigel, L. Gránásy, M. Tegze, and S. Pekker, Europhys. Lett. **32**, 721 (1995).

[36] W. I. F. David, R. M. Ibberson, T. J. S. Dennis, J. P. Hare, and K. Prassides, Europhys. Lett. **18**, 219 (1992).

[37] G. B. Adams, J. B. Page, O. F. Sankey, and M. O'Keeffe, Phys. Rev. B **50**, 17 471 (1994).

[38] M. Menon, K. R. Subbaswamy, and M. Sawtarie, Phys. Rev. B **49**, 13 966 (1994).

[39] D. Porezag, M. R. Pederson, Th. Frauenheim, and Th. Köhler, Phys. Rev. B **52**, 14 963 (1995).

[40] R. A. Jishi, R. M. Mirie, and M. S. Dresselhaus, Phys. Rev. B **45**, 13 685 (1992).

[41] J. Yu, L. Bi, R. K. Kalia, and P. Vashishta, Phys. Rev. B **49**, 5008 (1994).

[42] In what concerns the intensities we find (in the band 25–55 meV) the equivalent of $18\pm2$ degrees of freedom for $Rb_1C_{60}$, and $Rb_3C_{60}$, $21\pm2$ degrees of freedom for $Rb_6C_{60}$ and $17\pm2$ degrees of freedom for pristine $C_{60}$. The value for pristine $C_{60}$ corresponds to what we expect for the two $H_g$ plus one $T_{2u}$ and $G_u$ bands. The error stems from the incoherent approximation, which does not take into account the pronounced $Q$ dependence of the internal modes.

[43] L. Gránásy, T. Kemény, G. Oszlány, G. Bortel, G. Faigel, M. Tegze, S. Pekker, A. Jánossy, and L. Forró, Solid State Commun. **97**, 573 (1996).

[44] R. Zorn, A. Arbe, J. Colmenero, B. Frick, D. Richter, and U. Buchenau, Phys. Rev. E **52**, 781 (1995).

[45] M. C. Martin, D. Koller, X. Du, P. W. Stephens, and L. Mihály, Phys. Rev. B **49**, 10 818 (1994).

[46] M. Kosaka, K. Tanigaki, T. Tanaka, T. Atake, A. Lappas, and K. Prassides, Phys. Rev. B **51**, 12 018 (1995).

[47] H. Schober, B. Renker, F. Gompf, and P. Adelmann, Physica C **235-240**, 2487 (1994); B. Renker, F. Gompf, H. Schober, P. Adelmann, and R. Heid, J. Supercond. **7**, 647 (1994); H. Schober, B. Renker, and F. Gompf, Physica B **219-220**, 151 (1996).

[48] O. Zhou, J. E. Fischer, N. Coustel, S. Kycia, Q. Zhu, A. R. McGhie, W. J. Romanow, J. P. McCauley, Jr., A. B. Smith III, and D. E. Cox, Nature (London) **351**, 462 (1991).

[49] P. W. Stephens, L. Mihaly, P. L. Lee, R. L. Whetten, S. -M. Huang, R. Kaner, F. Deiderich, and K. Holczer, Nature (London) **351**, 632 (1991).

[50] R. D. Johnson, C. S. Yannoni, H. C. Dorn, J. S. Salem, and D. S. Bethune, Science **255**, 1235 (1992).